Available online at www.sciencedirect.com
SCIENCE DIRECT
Journal of Photochemistry and Photobiology A: Chemistry 180 (2006) 196–204
Journal of Photochemistry and Photobiology A:Chemistry
www.elsevier.com/locate/jphotochem

Fe^{3+}-TiO_2 photocatalysts prepared by combining sol–gel method with hydrothermal treatment and their characterization

Jiefang Zhu [a], Feng Chen [a], Jinlong Zhang [a,*], Haijun Chen [b], Masakazu Anpo [b]

[a] *Lab for Advanced Materials and Institute of Fine Chemicals, East China University of Science and Technology, 130 Meilong Road, Shanghai 200237, PR China*

[b] *Department of Applied Chemistry, Graduate School of Engineering, Osaka Prefecture University, 1-1 Gakuen-cho, Sakai, Osaka 599-8531, Japan*

Received 5 April 2005; received in revised form 2 September 2005; accepted 18 October 2005
Available online 22 November 2005

Abstract

Fe^{3+}-doped anatase nanosized TiO_2 photocatalysts have been prepared by combining sol–gel method with hydrothermal treatment. The samples were characterized by UV–vis diffuse reflectance spectroscopy, X-ray diffraction (XRD), Brunauer–Emmett–Teller (BET)-specific surface area (S_{BET}), transmission electron microscopy (TEM), atomic absorption flame emission spectroscopy (AAS), electron paramagnetic resonance (EPR) spectroscopy and X-ray photoelectron spectroscopy (XPS). From results of UV–vis diffuse reflectance spectroscopy, Fe^{3+}-doped TiO_2 extends its absorption to longer than 500 nm, which leads to an obvious photocatalatic activity under visible irradiation. From XRD, EPR, AAS and XPS, it was found that Fe exist in trivalent ionic state substituting Ti^{4+} in TiO_2 lattice and its concentration decreases from the surface to the center of doped TiO_2. The photocatalytic activity of prepared samples was investigated for the photocatalytic degradation of active yellow XRG dye. The photocatalytic activity of TiO_2 doped with appropriate content of Fe^{3+} exceeded those of non-doped TiO_2 and P25 both under UV and visible light irradiation.

Keywords: Titanium dioxide; Photocatalyst; Sol–gel method; Hydrothermal treatment; Doping; Fe^{3+}

1. Introduction

In recent years, titanium dioxide has been extensively used as an environmentally harmonious and clean photocatalyst, because of its various merits, such as optical and electronic properties, low cost, high photocatalytic activity, chemical stability and non-toxicity [1,2]. However, its practical application seems limited for several reasons, among which one is the low photon utilization efficiency, another is the need to use the ultraviolet (UV) as an excitation source. In order to solve these problems, the modification of these catalysts has also been attempted by doping them with various transition metals, including Fe^{3+}. Because the experimental conditions, preparation methods and standards for the evaluation of photocatalytic activity are usually different for various research groups, there are many argumentative results reported. Some research groups have reported that the presence of these foreign metal species in TiO_2 is generally detrimental for the degradation of organic compounds in aqueous systems [3–8], while some controversial results have been reported also [8–11].

Sol–gel method and impregnation technique have been employed to dope TiO_2 widely. By sol–gel method, solid–solution containing titanium and doping ion could be formed [12,13] and/or the doping ion could be incorporated into TiO_2 lattice [14], while as to doping iron into titania by impregnation technique, Fe_2TiO_5 or α-Fe_2O_3 can be easily produced on the surface of TiO_2 during calcination at high temperature [15]. In the former case, the dopant concentration is apt to excess in the bulk of TiO_2, then the possibility that a charge carrier meets a dopant increases and so does the chance of multiple trappings. If a charge carrier is trapped too many times in the bulk of TiO_2 or on its way to the surface, its apparent mobility may become extremely low and it will likely recombine with its mobile counterpart generated by subsequent photons before it can reach the surface [9]. In the latter case, the formation of Fe_2TiO_5 and α-Fe_2O_3 is disadvantageous, since their photocatalytic activity is

* Corresponding author. Tel.: +86 21 64252062; fax: +86 21 64252062.
E-mail address: jlzhang@ecust.edu.cn (J. Zhang).

1010-6030/$ – see front matter © 2005 Elsevier B.V. All rights reserved.
doi:10.1016/j.jphotochem.2005.10.017

poor and they occupy the effective surface sites for absorption and photocatalysis. No matter which method is employed, the control of the dopant amount seems very important. In addition, a rational distribution of dopant concentration may be the key to the effect of doping.

Hydrothermal method has been applied to synthesize nano-sized TiO_2 already, since products prepared by this method have well-crystalline phase and small crystallite size, which benefit to thermal stability and photocatalytic activity [16]. However, doping TiO_2 during hydrothermal crystallization has few reports. In present work, in order to optimize the distribution of dopant in TiO_2, doping TiO_2 with different amounts of Fe^{3+} was realized by combining sol–gel method with hydrothermal treatment. A systematic characterization was conducted. The photodegradation of active yellow XRG was chosen as a probe reaction to evaluate the photocatalytic activity of prepared samples. The relationship between structure and photoactivity of samples were proposed. A favorable distribution of dopant content was raised firstly.

2. Experimental

2.1. Preparation of doped TiO_2 photocatalysts

The doped TiO_2 photocatalysts were synthesized by combining sol–gel method with hydrothermal treatment. In sol–gel process, water and nitric acid were used to hydrolyze titanium *tert*-isopropoxide (TTIP, Acros +98%). 8 g TTIP was dissolved in 40 mL isopropanol. The mixture of 0.4 mL concentrated nitric acid ($\sim$14 mol L^{-1}), 30 mL water and 30 mL isopropanol was added to the TTIP solution, dropwise and with vigorous stirring. The resultant mixture was stirred for 2 h, aged for 1 day at room temperature and filtrated. Filter residue was rinsed with water and isopropanol repeatedly, dried at 343 K for 12 h in order to vaporize most of isopropanol and water, then the dried gels were crystallized and doped with Fe^{3+} as following: the 0.2 g dried gels and the required amount of $Fe(NO_3)_3{\cdot}9H_2O$ were mixed with 2.5 mL water and 25 mL isopropanol into a 160 mL PTFE-lined autoclave. The autoclave was heated to 473 K at a rate of 5 K min^{-1} and kept at 473 K for 8 h. Autogenous pressure gradually increased when the temperature was raised. After the hydrothermal treatment, the resulting powders were recovered by centrifugation, rinsed with diluted nitric acid and water repeatedly and dried at 353 K for 12 h. In this paper, the final samples will be denoted as xFe-TiO_2, where x indicates mass percentage of starting iron in theoretical product. For comparison, pure TiO_2 was also prepared without $Fe(NO_3)_3{\cdot}9H_2O$ in the same way. All chemicals were of analytical grade and used without further purification.

2.2. Characterization of Fe-TiO_2 photocatalysts

UV–vis diffuse reflectance spectra (DRS) were obtained for the dry-pressed disk samples using a scan UV–vis-NIR spectrophotometer (Varian Cary 500) equipped with an integrating sphere assembly, using $BaSO_4$ as reflectance sample. XRD measurements were carried out with a Rigaku D/max 2550 VB/PC apparatus at room temperature using Cu $K\alpha_1$ radiation (λ = 1.5406 Å) and a graphite monochromator, operated at 40 kV and 30 mA. The crystallite sizes of samples were determined at 40 kV and 200 mA and calculated from the half-height width of different diffraction peaks of anatase using Scherrer formula. High-purity silicon powder (99.9999%) was used as an internal standard to account for instrumental line broadening effect during crystal size estimation. The Brunauer–Emmett–Teller (BET)-specific surface areas (S_{BET}) of the samples were determined through nitrogen adsorption at 77 K (Micromeritics ASAP 2010). All the samples were degassed at 473 K before the measurement. For transmission electron microscopy (TEM) imaging, the sample powders were dispersed in isopropanol by 10 min ultrasonic irradiation and a drop of the suspension was placed onto a carbon-coated copper grid. The deposit was dried in air prior to imaging. The deposited particles were examined with a JEM-1200 EX II (JEOL Ltd.) transmission electron microscopy at an acceleration voltage of 120 kV. The X-band EPR spectra were recorded at 293 K using a Bruker ER 200D-SRC EPR spectrometer. The EPR spectrometer settings were: center field, 348.0 mT; scan range, 100.0 mT; modulation amplitude, 0.5 mT; scan time, 50 s; microwave frequency, 9.79 GHz; microwave power, 6.3 mW; spectrometer gain, 1.25×10^5. Experimental g values were determined with reference to a standard marker diphenyl picryl hydrazyl (DPPH), for which g = 2.0036. The actual content of Fe doped into TiO_2 was determined by atomic absorption flame emission spectroscopy (Shimadzu AA-6400F). To analyze the surface elemental composition and valent state of photocatalysts, X-ray photoelectron spectroscopy (XPS) was recorded with a Shimadzu ESCA-3200 spectrometer using a radiation source of Mg Kα radiation with the energy of 1253.6 eV, 30 mA × 8 kV. As an internal reference for the absolute binding energy, C 1s peak of 284.6 eV was used.

2.3. Photoactivity measurement

The photocatalytic activity of each sample was measured in terms of the degradation of active yellow XRG. The structure of XRG was shown in Scheme 1. XRG was selected because of well-defined optical absorption characteristic and good resistance to light degradation. 0.06 g of each catalyst was suspended in 60 mL of standard XRG aqueous solution (100 mg L^{-1}) using 70 mL capacity quartz tube. The catalysts were agitated for 1 h in XRG solution in the absence of light to attain the equilibrium adsorption on the catalyst surface. UV irradiation was carried out using a 300 W high-pressure Hg lamp, with the strongest emission at 365 nm, while the visible irradiation (>380 nm) was

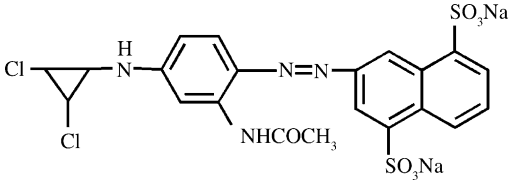

Scheme 1. Molecular structure of XRG.

achieved by cutting off the UV radiation of Hg lamp with a glass filter. The distance between the light and the reaction tube was 20 cm. The average light intensity striking the TiO_2 powder was about 1230 $\mu W\,cm^{-2}$, as measured by a UV radiometer (made in the Photoelectric Instrument Factory of Beijing Normal University) with the peak intensity of 365 nm.

After a given irradiation time, the samples of 3.5 mL were withdrawn and the catalysts were separated from the suspensions by filtration through 0.22 μm cellulose membranes. The quantitative determination of XRG was performed by measuring its absorption at 386 nm with a UV–vis spectrophotometer (Varian Cary 100). Each photodegradation experiment was repeated three times and the average was adopted. XRG was not photodegraded in the absence of any catalyst under the same irradiation condition. Moreover, no further degradation of XRG except limited absorption on the surface of the samples was observed in the dark. The photonic efficiency was calculated for each experiment as the ratio of the photocatalytic degradation rate and the incident photon flux. The determination of the total incident photon in the wavelength regions by chemical actinometry ferrioxalate [17] was performed in the same tube, which was used for all photocatalytic experiments, thus, avoiding the corrections for any influence of light reflection, beam position and reactor geometry.

An industrial pollutant 2,4-dichlorophenol (2,4-DCP), which does not absorb light in the visible spectral region, was also chosen to perform additional photocatalytic experiments with some synthesized samples. The experimental process is similar to the above one. The initial concentration of 2,4-DCP was 20 mg L^{-1}. The quantitative determination of 2,4-DCP was performed by measuring its absorption at 284 nm with the UV–vis spectrophotometer.

3. Results and discussion

The adsorption of NO_3^- on the surface of TiO_2 has been affirmed to be very weak in the previous studies [18,19]; therefore, $Fe(NO_3)_3$ was used in this work for the doping of Fe ions. XPS measurement also confirmed that the influence of NO_3^- could be neglected, for no nitrogen sign was observed in N 1s region of XPS spectra.

3.1. UV–vis diffuse reflectance spectra

UV–vis DRS of TiO_2 doped with Fe^{3+} are presented in Fig. 1. A steep increase of the absorption at shorter than 380 nm can be assigned to the intrinsic band gap absorption of pure anatase TiO_2 (~3.2 eV). In Fig. 1, Fe-TiO_2 shows enhanced absorptions in the range from 400 to 650 nm with the increasing Fe content, accompanied with the changes on color from white to reddish yellow. The enhanced absorptions in visible region may be contributed by two factors. One is the excitation of 3d electrons of Fe^{3+} to TiO_2 conduction band (charge transfer transition) at 415 nm, according to the energy levels proposed [20]. The other is a broad band centered at 500 nm, which can be ascribed to the d–d transition $^2T_{2g} \rightarrow {}^2A_{2g}$, $^2T_{1g}$ of Fe^{3+} or the charge transfer transition between iron ions ($Fe^{3+} + Fe^{3+} \rightarrow Fe^{4+} + Fe^{2+}$) [21].

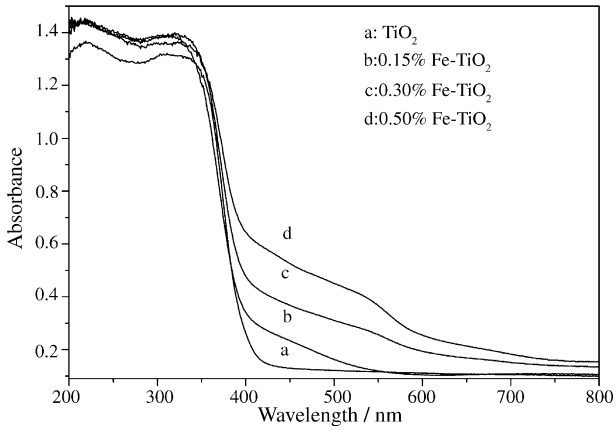

Fig. 1. UV–vis DRS of: (a) TiO_2; (b) 0.15% Fe-TiO_2; (c) 0.3% Fe-TiO_2; (d) 0.5% Fe-TiO_2.

3.2. X-ray diffraction

Fig. 2 shows XRD patterns of samples doped with Fe^{3+}. Within the detection limits of this technique, all samples consist of anatase (JCPDS 21–1272) as the unique phase. Any other crystalline phase containing Fe could not be observed, even at the highest Fe concentration. Full width half maximum (FWHM) of pattern peaks is broad indicating small crystal sizes for samples, of which the detailed data were showed in Table 1. Compared to pure TiO_2, the pattern peaks for Fe-doped TiO_2 slightly weaken and broaden. Since the radius of Fe^{3+} is 0.64 Å, which is a little smaller than 0.77 Å channels along the *c*-axis in pure TiO_2 and the radius of Ti^{4+} (0.68 Å) [22], it is possible that Fe^{3+} diffuses along the *c*-axis and substitutes Ti^{4+} in the TiO_2 lattice. Due to the different atomic sizes of Fe^{3+} and Ti^{4+}, some extent of deformation is introduced into the crystal lattice of TiO_2. Thus, comparing with the XRD pattern of net TiO_2, pattern peaks weakening were observed in those of Fe^{3+}-doped TiO_2. On the other hand, as a result of crystal lattice deformation, the crystallite growth of Fe^{3+}-doped TiO_2 grains is restrained during the hydrothermal treatment, which resulted in a slight broadening in XRD peaks.

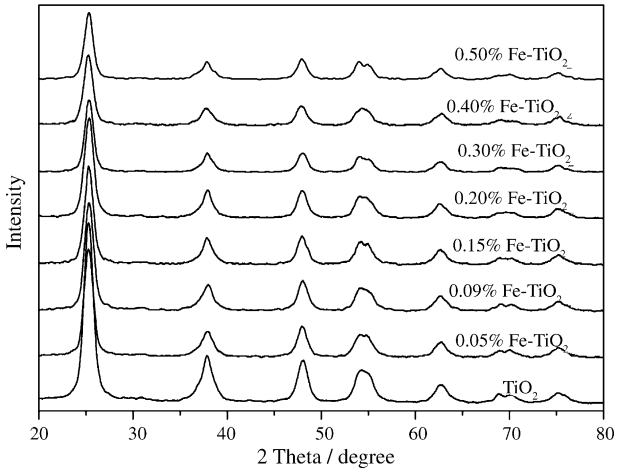

Fig. 2. XRD patterns of TiO_2 and Fe-TiO_2.

Table 1
Some characteristics and photocatalytic activity of samples prepared

Sample	Crystal size (nm)[a]	Crystal size (nm)[b]	S_{BET} ($m^2\ g^{-1}$)	Fe (wt%)[c]	UV-degraded XRG (%)[d]	ζ_{UV}[e] ($\times 10^{-5}$)	Vis-degraded XRG (%)[f]	ζ_{vis}[g] ($\times 10^{-5}$)
TiO_2	11.56	10.54	148.1	0	73.8	2.44	52.1	0.66
0.05% Fe-TiO_2	10.43	11.16	140.1	0.039	68.5	2.26	54.5	0.69
0.09% Fe-TiO_2	10.10	10.40	150.3	0.067	71.6	2.36	67.0	0.85
0.15% Fe-TiO_2	10.45	11.04	141.6	0.118	72.5	2.39	81.7	1.04
0.20% Fe-TiO_2	9.84	9.82	159.2	0.151	78.2	2.58	77.5	0.98
0.30% Fe-TiO_2	10.40	10.84	144.2	0.239	85.0	2.81	68.9	0.88
0.40% Fe-TiO_2	10.38	10.24	152.7	0.305	88.8	2.93	64.1	0.81
0.50% Fe-TiO_2	9.88	9.86	158.5	0.349	83.5	2.76	61.4	0.80

[a] Determined by XRD using Scherrer fomula.
[b] Calculated from S_{BET} assuming spherical particle morphology.
[c] Determined by atomic absorption flame emission spectroscopy.
[d] After photodegradation for 1 h, exclusive of equilibrium adsorption for 1 h. The value for P25 is 87.6%.
[e] ζ_{UV} is the average photonic efficiency during 1 h UV irradiation. The value for P25 is 2.89×10^{-5}.
[f] After photodegradation for 7 h, exclusive of equilibrium adsorption for 1 h. The value for P25 is 54.8%.
[g] ζ_{vis} is the average photonic efficiency during 7 h visible light irradiation. The value for P25 is 0.70×10^{-5}.

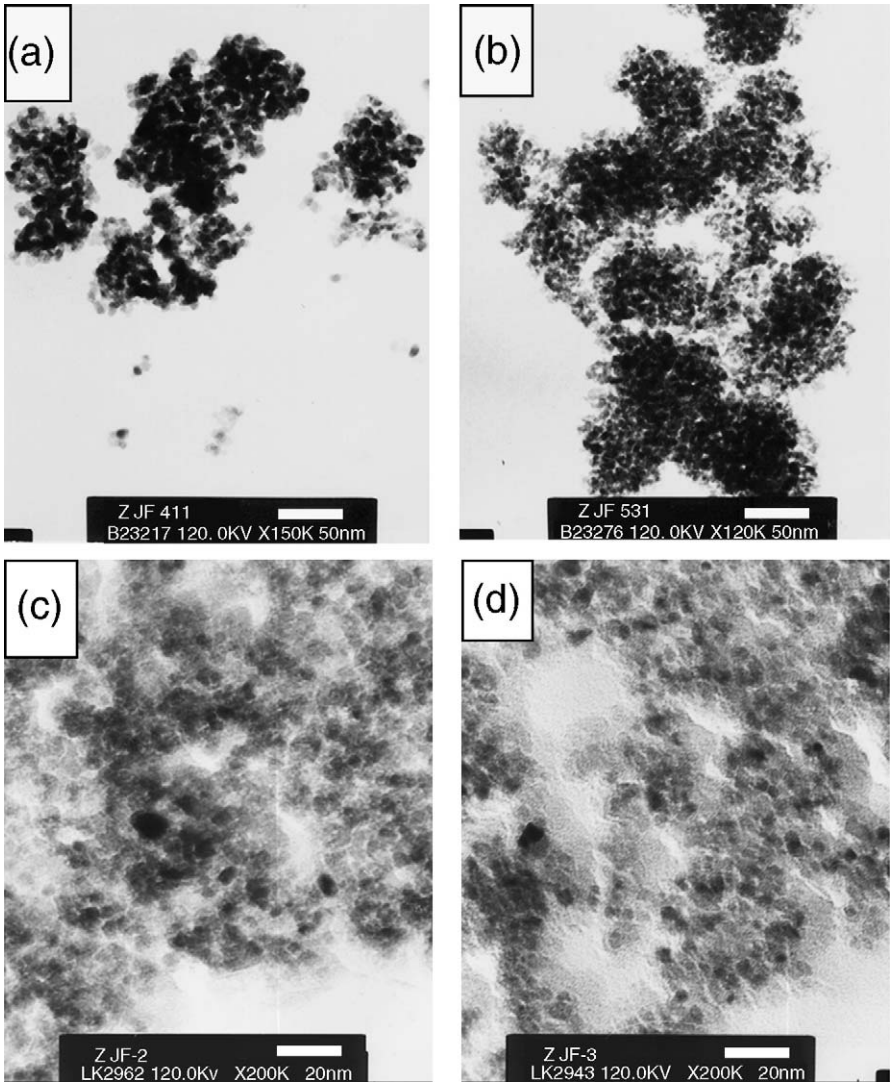

Fig. 3. TEM images of: (a) TiO_2; (b) 0.15% Fe-TiO_2; (c) 0.3% Fe-TiO_2; (d) 0.5% Fe-TiO_2.

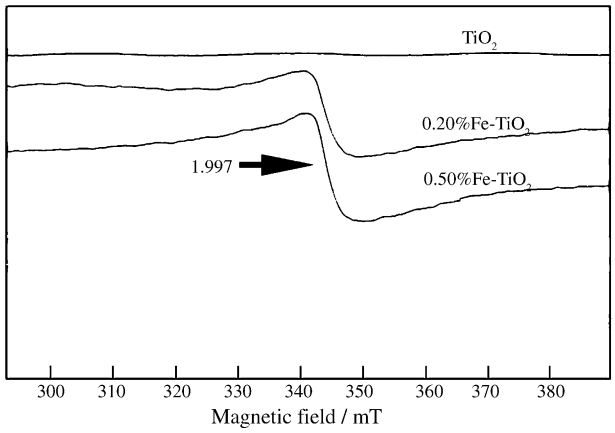

Fig. 4. EPR spectra of TiO_2, 0.2% Fe-TiO_2 and 0.5% Fe-TiO_2.

3.3. BET-specific surface area and TEM

All samples have large surface areas (140.1–159.2 $m^2\,g^{-1}$), which were little affected by doping, as shown in Table 1. TEM images of some samples are shown in Fig. 3. In Fig. 3, the primary grains are quite uniform in nearly spherical morphology and their sizes are consistent with those calculated from XRD measurement. The agglomerates formed by monodispersed primary particles can be clearly observed, with the sizes of 50–200 nm. These intraparticle pores have 8–11 nm average pore diameters and narrow pore size distributions, which were verified by N_2 adsorption–desorption isotherms and BJH pore size distribution (not shown here). According to the surface areas of samples and the density of anatase (3.84 $g\,cm^{-3}$), the calculated equivalent particle sizes are shown in Table 1, assuming spherical particle morphology. These calculated values match well with the grain sizes obtained by TEM and XRD, indicating agglomeration dose not markedly affect the surface areas of samples prepared with this method. Large surface area with mesoporous structure can promote adsorption, desorption and diffusion of reactants and products, which is favorable to obtain a high photocatalytic activity.

3.4. EPR spectra

The EPR spectra of some samples are shown in Fig. 4. EPR spectroscopy is the technique for detecting and monitoring very low levels of transition metal ion dopants and this highly sensitive technique can detect down to 0.01% of iron ions in metal oxide matrices [22]. From Fig. 4, Fe-TiO_2 have the signal of $g = 1.997$, which was assigned to Fe^{3+} spin ($S = 5/2$) in octahedral symmetry of anatase structure [23–25]. The spectrum of pure TiO_2 does not show any signal in this area. The intensities of EPR signal increase with Fe^{3+} content, while the broad line of pseudo-brookite does not exist even at the highest Fe content of 0.5%. These observations prove that the iron ions are mostly incorporated into the anatase crystal lattice by hydrothermal treatment.

3.5. Atomic absorption flame emission spectroscopy (AAS) and XPS studies

AAS and XPS were used to determine the total elemental composition, elemental surface composition and the electronic state of elements. The total elemental composition was shown in Table 1. From Table 2, the atomic concentration ratios of O 1s to Ti 2p are far greater than 2.0 in all samples, indicating that the surfaces are hydrated and/or hydroxylated, which are also verified by FTIR (not shown here). A high content of surface hydroxyl groups and adsorbed water may be a distinct property of hydrothermal specimens [26]. From Tables 1 and 2, it is obvious that for Fe dopant, the actual bulk Fe^{3+} content determined by AAS is a little lower than the nominal one and far lower than surface Fe^{3+} content determined by XPS. It can be supposed that firstly Fe^{3+} can be adsorbed mostly and strongly on the surface of TiO_2 dried gels due to their very large surface area and strong electrostatic interaction and then Fe^{3+} may diffuse gradually into the bulk at given temperature and pressure during hydrothermal crystallization. Therefore, the content of Fe^{3+} decreases in the direction of the diffusion, from the exterior to the interior.

XPS spectra of some Fe-TiO_2 are shown in Fig. 5. Peaks at around 284.6 eV are found in all survey spectra, corresponding to carbon impurities, arising probably from the background of XPS test or the residual precursors. The Ti $2p_{1/2}$ and Ti $2p_{3/2}$ spin-orbital splitting photoelectrons for all Fe-TiO_2 samples are located at binding energies of 464.2 and 458.5 eV, respectively, which are in excellent agreement with the values of Ti^{4+} in pure TiO_2 [27], as seen in Fig. 5b. These energies seem not affected by doping iron ion. Perhaps, due to the low concentration of iron ion, the shift of Ti 2p peaks is below the detection limit. No Ti^{3+} species were observed in XPS. No broad FWHM of Ti $2p_{3/2}$ signals, about 1.4 eV for all samples may also indicate the only presence of Ti^{4+} species [28] and well crystallization for all samples [29]. Fig. 5c shows the O 1s core level spectra of Fe-TiO_2. The peaks at 530.1 eV for all Fe-TiO_2 are due to O^{2-} ion in the TiO_2 lattice. In the spectra of 0.15% Fe-TiO_2, 0.30% Fe-TiO_2 and 0.50% Fe-TiO_2, a shoulder to the main O 1s peak at higher binding energy is obvious, which should be attributed to the surface hydroxyl groups or chemisorbed water molecules on the titania [29,30]. The O 1s spectrum of 0.09% Fe-TiO_2 even shows a second peak located at a binding energy of 532.5 eV. Thus, 0.09% Fe-TiO_2 contains more surface hydroxyl groups or chemisorbed water molecules, in well agreement with the higher atomic ratio of O to Ti in Table 2. The signals of Fe are weak, due to the low doping level. The binding energies from 711.0 to 711.8 eV and from 725.4 to 726.0 eV should be assigned to $2p_{3/2}$

Table 2
Elemental surface composition determined by XPS

Sample (% Fe-TiO_2)	Ti 2p (at%)	O 1s (at%)	Fe 2p (at%)
0.09	13.93 (32.6)	85.97 (67.2)	0.10 (0.3)
0.15	18.50 (40.2)	81.20 (59.0)	0.30 (0.8)
0.30	17.35 (38.1)	82.00 (60.2)	0.65 (1.7)
0.50	14.71 (33.6)	84.66 (64.7)	0.63 (1.7)

Values in parentheses are in wt%.

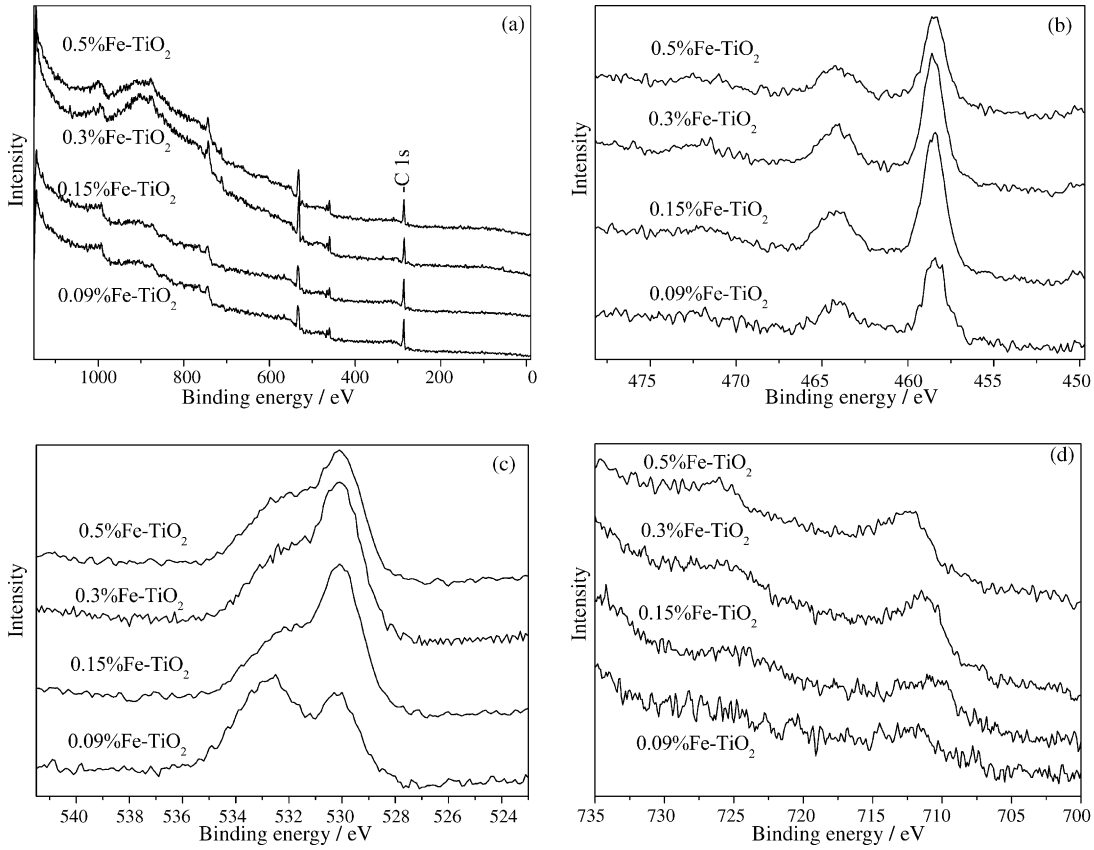

Fig. 5. XPS spectra of some Fe-TiO_2: (a) survey; (b) Ti 2p peaks; (c) O 1s peaks; (d) Fe 2p peaks.

and $2p_{1/2}$ of Fe^{3+}, respectively. These data exhibit a positive shift compared to those in Fe_2O_3 (710.7 eV for $2p_{3/2}$ and 724.3 eV for $2p_{1/2}$) [27], probably indicative of more positively charged surface Fe^{3+}. The slight enhancement of Fe 2p level binding energy may be due to the diffusion of Fe^{3+} into TiO_2 lattice and the formation of Fe–O–Ti bond in the samples.

3.6. Photocatalytic activity

The photocatalytic activity of samples prepared and P25 was determined by the photocatalytic degradation of XRG under UV or visible light irradiation, as shown in Figs. 6–8 and Table 1. In Figs. 6 and 7, C_0 and C are the initial concentration after the equilibrium adsorption and the reaction concentration of XRG, respectively. For the clearness of these figures, only representative curves are selected. In Fig. 6, high efficient degradation is apt to exhibit pseudo-first-order kinetics, while slower degradation preferably obeys pseudo-zero-order kinetics, which may be dominated by electron–hole recombination [31]. In Fig. 7, all the photocatalytic degradation follows pseudo-zero-order kinetics, maybe due to slow degradation rates. In Fig. 7, at the first hour after photocatalytic degradation, C is higher than C_0 for some samples, which may arise from desorption of XRG induced by irradiation. From Table 1 and Figs. 6–8, most Fe-TiO_2 have higher photocatalytic activity than pure TiO_2 both under UV and visible light irradiation. The optimal Fe^{3+} doping level is 0.4% for the degradation of XRG under UV light irradiation, in which case the phocatalytic activity is even a little higher than that of P25, a well known commercial photocatalyst of high photoactivity, while 0.15% is the optimal Fe^{3+} doping content for the degradation of XRG under visible light excitation. The difference in the optimal Fe^{3+} doping content is mostly because of the different photoactive enhancement effect in the two exciting cases.

Colorless 2,4-DCP solution was also photodegraded by some typical samples. In this process, the sensitization of dye under visible light irradiation can be excluded. Due to the lower photonic efficiencies in Table 3, the 2,4-DCP was proved much

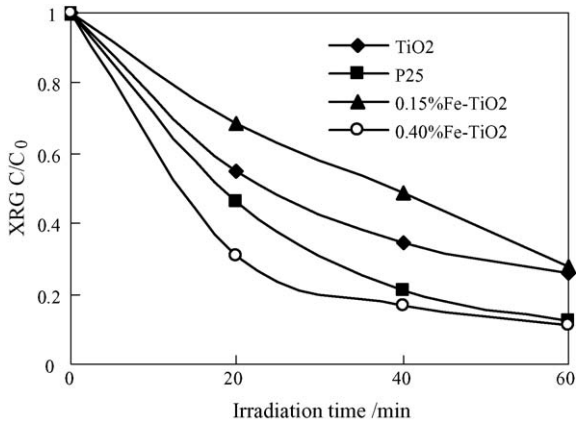

Fig. 6. Photodegradation of XRG by some Fe-TiO_2 as a function of UV light irradiation time.

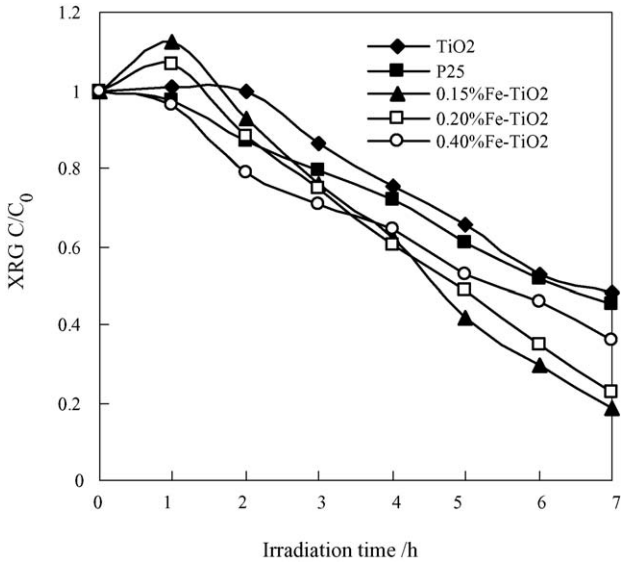

Fig. 7. Photodegradation of XRG by some Fe-TiO_2 as a function of visible light irradiation time.

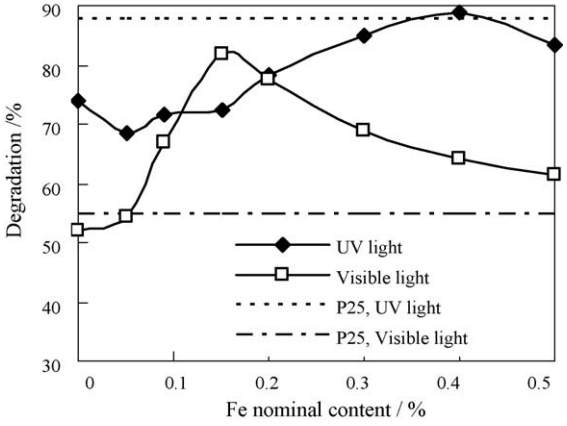

Fig. 8. Photodegradation of XRG by Fe-TiO_2 as a function of doping concentration. UV and visible light irradiation times were 1 and 7 h, respectively.

more stable than XRG under photocatalysis. However, the effect from doping is still obvious as XRG photocatalysis. The 0.40% Fe-TiO_2 is more photoactive than TiO_2 and P25 under UV irradiation, while 0.15% Fe-TiO_2 is more effective than TiO_2 and P25 under visible light irradiation. These results confirm the photocatalytic activity of the prepared Fe-TiO_2, especially activity under visible light irradiation.

The high photocatalytic activity of samples prepared by present method may be ascribed to small crystal size, high specific surface area, mesoporous structure, as well as surface chemisorbed water and hydroxyl groups, which can react with photogenerated holes to produce hydroxyl radicals. From XPS studies, it can be concluded that doping benefits to the absorption of water and hydroxyl groups. Doping of Fe^{3+} has been affirmed to introduce much more oxygen vacancies in/on the crystal lattice and surface of TiO_2, while oxygen vacancies favor the adsorption of H_2O and formation of surface hydroxyl group, as well as promote the photocatalytic activity. The beneficial effect of Fe^{3+} could be further explained by considering the efficient separation of photoexcited electrons and holes. Fe^{3+} can act as photogenerated hole trappers (Eq. (2)), due to the energy levels for Fe^{3+}/Fe^{4+} above the valence band edge of anatase TiO_2 [8,21]. The trapped holes in Fe^{4+} can migrate to the surface adsorbed hydroxy ion (Eq. (3)) to produce hydroxyl radical:

$$TiO_2 + h\nu \rightarrow e_{cb}^- + h_{vb}^+ \quad (1)$$

$$Fe^{3+} + h_{vb}^+ \rightarrow Fe^{4+} \quad (2)$$

$$Fe^{4+} + OH^- (ads) \rightarrow Fe^{3+} + OH^\bullet (ads) \quad (3)$$

In addition, for the charge compensation for electroneutrality in doped TiO_2, O^{2-} in the surface lattice can easily escape to trap photogenerated holes (Eqs. (4) and (5)) and produce hydroxyl radicals (Eq. (6)):

$$O^{2-} + h_{vb}^+ \rightarrow O^- \quad (4)$$

$$O^- + h_{vb}^+ \rightarrow O^\bullet \quad (5)$$

$$O^- + H_2O (ads) \rightarrow OH^\bullet (ads) + OH^- (ads) \quad (6)$$

Fe^{3+} can also serve as photogenerated electron trappers (Eq. (7)), which has been supported by EPR elsewhere [23]. Subsequently, Fe^{2+} could be oxided to Fe^{3+} by transferring electrons to absorbed O_2 on the surface of TiO_2 (Eq. (8)) and a neighboring surface Ti^{4+} (Eq. (9)), which then lead to interfacial electron transfer (Eq. (10)) [8]:

$$Fe^{3+} + e_{cb}^- \rightarrow Fe^{2+} \quad (7)$$

$$Fe^{2+} + O_2 (ads) \rightarrow Fe^{3+} + O_2^- \quad (8)$$

$$Fe^{2+} + Ti^{4+} \rightarrow Fe^{3+} + Ti^{3+} \quad (9)$$

$$Ti^{3+} + O_2 (ads) \rightarrow Ti^{4+} + O_2^- \quad (10)$$

Furthermore, Fe^{3+} is relatively stable due to its $3d^5$ (half-filled high spin) electronic configuration and the trapped charge can easily release from Fe^{2+} or Fe^{4+} to return back to Fe^{3+} ($3d^5$) and then migrate to the surface to participate in photocatalytic reaction.

Unfortunately, Fe^{3+} can also act as the recombination centers for the photogenerated electrons and holes, according to two pairs of reactions (Eqs. (2), (7) and (11)–(13)). When the dopant concentration is too high, the recombination rate will increase and compete with the redox processes because the distance between trapping sites decreases.

$$Fe^{4+} + e_{cb}^- \rightarrow Fe^{3+} \quad (11)$$

$$Fe^{2+} + h_{vb}^+ \rightarrow Fe^{3+} \quad (12)$$

Table 3
Photonic efficiencies of 2,4-DCP photocatalytic degradation by some samples

	P25	TiO_2	0.15% Fe-TiO_2	0.40% Fe-TiO_2
ζ_{UV}[a] ($\times 10^{-5}$)	1.85	1.67	1.74	2.09
ζ_{vis}[b] ($\times 10^{-6}$)	5.12	4.98	8.36	7.06

[a] ζ_{UV} is the average photonic efficiency during 1 h UV irradiation.
[b] ζ_{vis} is the average photonic efficiency during 7 h visible light irradiation.

$$Fe^{2+} + OH^{\bullet} \rightarrow Fe^{3+} + OH^{-} \quad (13)$$

The reactions corresponding to Eqs. (3)–(6) and (8)–(10) occur on the surface of doped TiO_2 and arise from doping, that is to say, all the interfacial charge transfer reactions involving Fe^{3+} are valid only when Fe^{3+} are located close to the surface sites, so the surface content of Fe^{3+} should not be too less. On the other hand, in order to reduce the possibility of multiple trappings, the dopant concentration in the bulk should not be too high [9]. The distribution of Fe^{3+} in prepared samples may meet these requirements. The degressive content of dopant, from the exterior to the interior, may result in high photocatalytic activity. As we know, iron ions were uniformly distributed in the interstices of titania crystals to form a titanium–iron solid–solution when the samples were calcined at 80, 200 and 400 °C for the Fe doping TiO_2 photocatalyst prepared by ordinary sol–gel method [12]. Therefore, their photocatalytic activity cannot been enhanced so obviously under UV or visible irradiation. It is possible reason that Fe^{3+} was doped uniformly from the exterior to the interior by sol–gel method.

A more evidently enhancement on the photocatalytic activity of doped TiO_2 was observed under visible irradiation than that under UV irradiation, as shown in Fig. 8. Different with the intrinsic excitation of TiO_2 under UV irradiation, the excitation behavior of doped TiO_2 under visible irradiation is suggested involving the Fe^{3+} ion. The t_{2g} level of 3d orbital of Fe^{3+} is above the valence band of TiO_2, which can absorb a photon with a wavelength around 415 nm to produce a Fe^{4+} ion and a TiO_2 conductive band electron (Eq. (14)). Conductive band electrons react with adsorbed O_2 to form O_2^- (Eq. (15)), while Fe^{4+} reacts with surface hydroxyl group to produce hydroxyl radical. Therefore, XRG was photodegraded even under the visible light irradiation. Another additional possible reason is the photo-induced electron transfer transition between Fe^{3+} themselves, which results in a broad absorption around 500 nm and produces Fe^{2+} and Fe^{4+}. Fe^{2+} and Fe^{4+} then react with O_2 and surface hydroxyl group to produce O_2^- and hydroxyl radical, which degrade XRG:

$$Fe^{3+} + h\nu \rightarrow Fe^{4+} + e_{cb}^{-} \quad (14)$$

$$e_{cb}^{-} + O_2 \rightarrow O_2^{-} \quad (15)$$

4. Conclusion

Iron-doped titanium dioxide photocatalysts were prepared by the combination of sol–gel process with hydrothermal treatment. Photocatalysts prepared by this method have high specific surface areas, small crystal sizes, mesoporous structure, as well as a large amount of surface adsorbed water and hydroxyl groups, which contribute to their high photocatalytic activity. It was found that Fe^{3+} doping content decrease from the surface to the core. This distribution of dopants may be in favor of the interfacial charge transfer reactions. Fe^{3+} can help the separation of photogenerated electrons and holes by trapping them temporarily and shallowly. Iron-doped titanium dioxide photocatalysts also can absorb and utilize the visible light to photocatalyze the degradation of XRG, due to the excitation of 3d electron of Fe^{3+} to the conduction band of TiO_2 and the electron transfer transition between Fe^{3+} themselves.

Acknowledgments

This work has been supported by Program for New Century Excellent Talents in University (NCET-04-0414); the National Basic Research Program of China (2004CB719500); Shanghai Nanotechnology Promotion Center (0452nm010); National Nature Science Foundation of China (20407007).

References

[1] M.R. Hoffmann, S.T. Martin, W. Choi, D.W. Bahnemann, Chem. Rev. 95 (1995) 69.
[2] A. Fujishima, T.N. Rao, D.A. Truk, J. Photochem. Photobiol. C Photochem. Rev. 1 (2000) 1.
[3] A. Di Paola, G. Marcì, L. Palmisano, M. Schiavello, K. Uosaki, S. Ikeda, B. Ohtani, J. Phys. Chem. B 106 (2002) 637.
[4] J.A. Navío, J.J. Testa, P. Djedjeian, J.R. Padrón, D. Rodríguez, M.I. Litter, Appl. Catal. A Gen. 178 (1999) 191.
[5] M. Anpo, M. Takeuchi, J. Catal. 216 (2003) 505.
[6] B. Pal, T. Hata, K. Goto, G. Nogami, J. Mol. Catal. A Chem. 169 (2001) 147.
[7] H. Kato, A. Kudo, J. Phys. Chem. B 106 (2002) 5029.
[8] W. Choi, A. Termin, M.R. Hoffmann, J. Phys. Chem. 98 (1994) 13669.
[9] Z. Zhang, C. Wang, R. Zakaria, J.Y. Ying, J. Phys. Chem. B 102 (1998) 10871.
[10] H. Yamashita, M. Harada, J. Misaka, M. Takeuchi, K. Ikeue, M. Anpo, J. Photochem. Photobiol. A Chem. 148 (2002) 257.
[11] J. Araña, O.G. Díaz, M.M. Saracho, J.M.D. Rodríguez, J.A.H. Melián, J.P. Peña, Appl. Catal. B Environ. 36 (2002) 113.
[12] J.A. Wang, R. Limas-Ballesteros, T. López, A. Moreno, R. Gómez, O. Novaro, X. Bokhimi, J. Phys. Chem. B 105 (2001) 9692.
[13] J.A. Navío, G. Colón, M. Macías, C. Real, M.I. Litter, Appl. Catal. A Gen. 177 (1999) 111.
[14] Z. Wang, G. Yang, P. Biswas, W. Bresser, P. Boolchand, Powder Technol. 114 (2001) 197.
[15] J.A. Navío, G. Colón, M. Trillas, J. Peral, X. Domènech, J.J. Testa, J. Padrón, D. Rodríguez, M.I. Litter, Appl. Catal. B Environ. 16 (1998) 187.
[16] H. Kominami, J. Kato, Y. Takada, Y. Doushi, B. Ohtani, S. Nishimoto, M. Inoue, T. Inui, Y. Kera, Catal. Lett. 46 (1997) 235.
[17] S.L. Murov, Handbook of Photochemistry, Marcel Dekker Inc., New York, 1973, pp. 119–123.
[18] K. Bourikas, T. Hiemstra, W.H. Van Riemsdijk, Langmuir 17 (2001) 749.
[19] M. Andersson, L. Österlund, S. Ljungström, A. Palmqvist, J. Phys. Chem. B 106 (2002) 10674.
[20] T. Umebayashi, T. Yamaki, H. Itoh, K. Asail, J. Phys. Chem. Solids 63 (2002) 1909.
[21] J. Zhu, W. Zheng, B. He, J. Zhang, M. Anpo, J. Mol. Catal. A Chem. 216 (2004) 35.
[22] T.A. Egerton, E. Harris, E.J. Lawson, B. Mile, C.C. Rowlands, Phys. Chem. Chem. Phys. 3 (2001) 497.
[23] J. Soria, J.C. Conesa, V. Augugliaro, L. Palmisano, M. Schiavello, A. Sclafani, J. Phys. Chem. 95 (1991) 274.
[24] Y. Zhang, S.G. Ebbinghaus, A. Weidenkaff, T. Kurz, H.-A.K. von Nidda, P.J. Klar, M. Güngerich, A. Reller, Chem. Mater. 15 (2003) 4028.
[25] A. Amorelli, J.C. Evans, C.C. Rowlands, T.A. Egerton, J. Chem. Soc. Faraday Trans. I 83 (1987) 3541.
[26] J.M. Coronado, A.J. Maira, J.C. Conesa, K.L. Yeung, V. Augugliaro, J. Soria, Langmuir 17 (2001) 5368.

[27] C.D. Wagner, W.M. Riggs, L.E. Davis, J.F. Moulder, G.E. Muilenberg, Handbook of X-Ray Photoelectron Spectroscopy, Perkin-Elmer Corp., Physical Electronics Division, USA, 1979.
[28] W. Zhang, Y. Li, S. Zhu, F. Wang, Chem. Phys. Lett. 373 (2003) 333.
[29] K. Nagaveni, M.S. Hegde, N. Ravishankar, G.N. Subbanna, G. Madras, Langmuir 20 (20042900).
[30] B. Erdem, R.A. Hunsicker, G.W. Simmons, E.D. Sudol, V.L. Dimonie, M.S. El-Aasser, Langmuir 17 (2001) 2664.
[31] A.-W. Xu, Y. Gao, H.-Q. Liu, J. Catal. 207 (2002) 151.